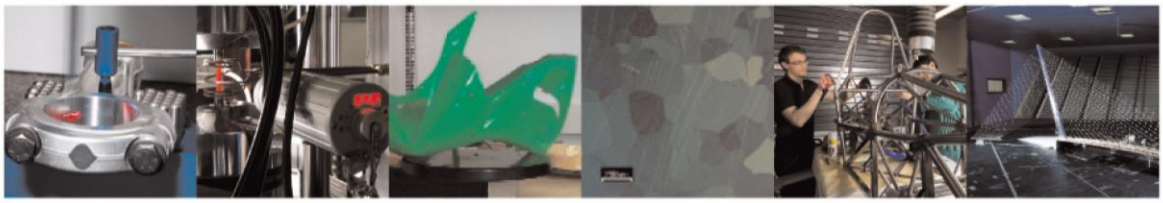

# Micro laser metal wire deposition for additive manufacturing of thin-walled structures

Demir, Ali Gökhan

This is a post-peer-review, pre-copyedit version of an article published in OPTICS AND LASERS IN ENGINEERING. The final authenticated version is available online at: http://dx.doi.org/10.1016/j.optlaseng.2017.07.003

# Micro laser metal wire deposition for additive manufacturing of thin-walled structures

Ali Gökhan Demir[1]*

[1]Department of Mechanical Engineering, Politecnico di Milano, Via La Masa 1, 20156 Milan, Italy

*Corresponding author; aligokhan.demir@polimi.it

**Micro laser metal wire deposition for additive manufacturing of thin-walled structures**

Ali Gökhan Demir[1]*

[1]Department of Mechanical Engineering, Politecnico di Milano, Via La Masa 1, 20156 Milan, Italy

*Corresponding author; aligokhan.demir@polimi.it

**Abstract**

In this work, the micro laser metal wire deposition (µLMWD) process is studied as an additive manufacturing process for manufacturing thin walled structures with high aspect ratio. The developed µLMWD system consisted of a flash-pumped Nd:YAG laser source operating with ms-long pulses and an in-house developed wire feeding system. Processing conditions were investigated for single and multi-layer deposition in terms of geometry, microhardness and material use efficiency. Thin-walled structures with aspect ratio up to 20 were manufactured successfully, where layer width was between 700 and 800 µm. In multi-layer deposition conditions, the material use efficiency was observed to be close to 100%. The microhardness over the build direction was homogenous. The results show that the µLMWD process yields geometrical resolution close to powder-bed additive manufacturing processes, while maintaining the benefits of using wire feedstock.

**Keywords:** Additive manufacturing; micro components; wire feeding system; directed energy deposition

## 1. Introduction

Additive manufacturing of metallic components employing a metallic wire feedstock falls within the directed energy deposition (DED) process family [1]. The process consists of the feed of the metallic wire that is melted by a heat source, which are manipulated over the deposition volume [2]. The use of metallic wire as the feedstock material in additive manufacturing processes provides several advantages compared to powder precursors. Compared to powder precursors, they are easier to stock and most commonly easier to produce. Several heat sources are available for the melting of the wire feedstock such as plasma, arc, electron beam and laser [2–4]. The process precision and build rate depend highly on the employed heat source, where electron beam and laser stand out as heat sources with higher precision. Wire based metal additive manufacturing processes take further advantage of high deposition rates and efficient use of feedstock. Powder-bed processes such as selective laser melting (SLM) and electron beam melting (EBM) require the filling of the whole process volume by the powder, which is later on selectively melted [5]. Although most of the powder can be recycled,

the necessity of filling the build volume becomes problematic when large components should be produced. Material losses occur due to non-recyclable portion of the powder, which is contaminated within the during the melting process. Reactive powders such as Ti and Al alloys can get oxidised in use and in recycling, degrading the manufacturing quality over time [6]. In DED processes with powder feedstock, the need for filling the work volume with powder is avoided and the overall build rates are higher. However, powder recovery and recycling remain problematic.

From this point view DED processes based on wire feedstock are appealing as they unite the benefits of high deposition rates, high material use efficiency, and possibility operate in large volumes. Accordingly, they have found applications in manufacturing of large component and axisymmetric parts. On the other hand, these processes lack dimensional resolution in terms of smallest dimensions of layer thickness and width achievable. Powder-bed processes benefit from the small dimensions of the powder size (typically between 15-40 µm), small layer thicknesses (20-50 µm) and small laser beam sizes (30-100 µm). Lattice structures and thin walls are achievable with powder-bed processes thanks to these dimensional features [7],[8]. A wire feed DED process with similar dimensional capabilities would be beneficial for several applications that require increased dimensional resolution with the flexibility of manipulation provided by the wire feed-stock. One of the most important applications is additive manufacturing in space, where powder management becomes much more difficult in microgravity.

In order to reduce the geometrical features of a wire feed DED system, one of the key aspects is the use of thin wires. Most of the previous works in literature involves the use of wire diameters around 1 mm. Commonly the deposit width is 5 to 15 times the wire diameter, which further decreases the geometrical resolution [9–13]. The final deposition width depends on the used heat source characteristics and process parameters. As most of the research concentrated around higher deposition rates, solutions for micro wire DED have received much less attention. Accordingly, the processes are characterised by a layer height varying in a large range between 2 to 19 mm and wall widths between 3 to 16 mm [14],[15]. Jhavar et al [16] in particular proposed a micro plasma transferred arc (µPTA) wire deposition process with 0.3 mm diameter AISI P20 tool steel, in which layer height was between 0.5 to 0.7 mm, wall width varied was approximately 2 mm. Previously reported processes commonly involve the use of arcs as heat sources, whereas the use of lasers can provide a better solution in terms of limiting the heat source extension. In particular, pulsed wave (PW) emission would

allow for a more precise control over the deposited over time. Long pulsed lasers operating with ms-long pulses are suitable for this operation, where heat input can be regulated better compared to continuous wave (CW) lasers [17]. A micro wire DED process employing a laser would not necessarily require high intensities due to the used thin wire. Operating in processing conditions similar to conduction welding would be suitable, where material loss due to vaporization can also be avoided. Laser beam diameter can be comparable to the wire size allowing for correct positioning of the heat source over the deposited wire [18].

Therefore, this work develops and investigates the micro laser metal wire deposition (μLMWD) process. In particular, the process development for obtaining thin-walled structures is shown. The work describes the system development and a carries a detailed experimental work depicting the process capabilities in terms of the achievable dimensions and material use efficiency with a 0.5 mm diameter AISI 301 stainless steel wire. The influence of process parameters over the single layer deposition is investigated. Multi-layer deposition is analysed for building thin-walled structures with high aspect ratio. Material mechanical properties are investigated through microhardness measurements. Finally, demonstrator cases are presented over different thin-walled geometries.

## 2. Materials and methods

### 2.1. Material

Both substrate and wire materials were austenitic stainless steels. AISI 301 wires with 0.5 mm diameter were used throughout the study together with 10 mm-thick AISI 316 substrates. The wire material is characterised by good formability and cold workability rendering it suitable for wire production and possesses good weldability [19].

**Table 1. Nominal chemical composition of the wire and substrate materials** [19]**.**

| wt% | C | Si | Mn | P | S | Cr | Mo | Ni | Fe |
|---|---|---|---|---|---|---|---|---|---|
| AISI 301 | 0.15 | 0.75 | 2 | 0.045 | 0.03 | 16-18 | | 6-8 | Bal. |
| AISI 316 | 0.08 | 0.75 | 2 | 0.045 | 0.03 | 16-18 | 2-3 | 10-14 | Bal. |

### 2.2. μLMWD system

The μLMWD system composed of a welding station (Powerweld HL 124P from Trumpf, Ditzingen, Germany) and in-house built wire feeder. The welding station was equipped with a Nd:YAG source, producing μs to ms pulses with at Hz-level pulse repetition rates (*PRR*). Maximum peak power ($P_{peak}$) available to the

pulses is 5 kW and resultant maximum average power and pulse energy ($E$) are 120 W and 50 J respectively. Fiber delivery is used to transport the laser beam from the source to the processing head. The system is equipped with 0.4 mm fiber, 200 mm collimating and 150 mm focal lenses producing a minimum spot diameter of 0.3 mm. The optical chain can be automatically adjusted to vary the spot diameter between 0.3 and 0.5 mm. The welding station is equipped with 3 linear and 1 rotational axis, whose speed ($v$) is controlled through numerical control of the system. The wire feeder system namely Lachesis was controlled through a Labview interface, regulating the wire feed rate (WFR) and synchronising the laser emission at the start of each new layer. The system used different nozzle dimensions to accommodate different wire sizes.

Within the μLMWD process, wire feed direction and wire feeding angle were set by the position of the wire feeder with respect to the substrate and deposition direction. Shielding gas type and pressure were set through the numerical control of the welding station. Within the process laser pulse energy ($E$), pulse duration ($\tau$) and pulse repetition rate were regulated to manage the heat input.


**Figure 1. Details of the μWLMD system. a) Overview of the welding station and the laser source. b) Lachesis wire feeder implemented inside the welding station. c) Image of the process obtained through the viewing system coupled to the optical chain. d) Deposition of a thin-walled structure with the system.**

**Table 2. Main characteristics of the prototype μWLMD system.**

| Parameter | Value |
|---|---|
| Laser system | Trumpf PowerWeld HL 124P |
| Laser type | Flash pumped Nd:YAG |
| Emission wavelength ($\lambda$) | 1064 nm |
| Max average power ($P_{avg}$) | 120 W |
| Max peak power ($P_{pk}$) | 5 kW |
| Max pulse energy ($E$) | 50 J |
| Pulse duration ($\tau$) | 0.3-20 ms |
| Pulse repetition rate ($PRR$) | 1-300 Hz |
| Beam parameter product ($BPP$) | 16 mm·mrad |
| Min. beam diameter ($d_0$) | 300 μm |
| Maximum wire feed rate ($WFR$) | 900 mm/min |
| Wire diameter ($d_w$) | 0.3-0.5 mm |

### 2.3. Characterization

Cross-sections of single-layer deposits and multi-layer thin walls were made by abrasive saw cutting and abrasive paper polishing. Samples were later etched to reveal microstructure with Nital solution. Optical microscopy images were taken (Leitz Ergolux 200 from Leica, Wetzlar, Germany). Multi-layered thin wall structure dimensions were measured with coordinate measuring machine (CMM, Prismo 5 VAST MPS HTG from Carl Zeiss, Oberkochen, Germany). Vickers microhardness was measured over the cross sections with 500 gf applied load and 15 s dwell time (VMHT 30A from Leica, Wetzlar, Germany).

### 2.4. Evaluation of material use efficiency

One of the important factors regarding the use of wire for additive manufacturing is the efficient use of the precursor material. In powder based additive manufacturing processes re-use of powder is possible after adequate sieving operations. Powder-bed based selective laser melting process requires large quantity of powder to sustain the build components also on the non-built regions. In laser metal deposition, non-adhered powder can be lost reducing the overall efficiency of the material use [20]. In wire based directed energy deposition processes material loss can be mainly due to the generation of sparks, dross and fumes. Beyond economic reasons, evaluation of the material use efficiency is important also for waste management [21]. High efficiency in material use is another indicator to process stability, which is crucial for maintaining geometrical tolerances. Material use efficiency ($\eta$) can be calculated as the proportion of deposited volume ($V_d$) to the delivered wire volume ($V_w$).

$$\eta = \frac{V_d}{V_w} \quad (1)$$

Delivered wire volume depends on process parameters namely wire diameter ($d_w$), wire feed rate (*WFR*), number of layers (*N*) and the duration of a single layer (*t*). For a thin-walled structure developed on a constant length (*l*) and with constant transversal speed (*v*) deposited wire volume can be calculated as:

$$V_w = \frac{\pi}{4} \cdot {d_w}^2 \cdot WFR \cdot t \cdot N = \frac{\pi}{4} \cdot {d_w}^2 \cdot WFR \cdot \frac{l}{v} \cdot N \quad (2)$$

Considering a constant deposited section ($A_d$) over the total deposited length (*l*), the material use efficiency can be calculated as the following

$$\eta = \frac{A_d}{\frac{\pi}{4} \cdot {d_w}^2 \cdot WFR \cdot \frac{1}{v} \cdot N} \quad (3)$$

Accordingly, the deposited material area was measured for both single and multi-layer deposits to estimate the corresponding material use efficiency.

### 2.5. Experimental plan

The main aim of the experimental work was to demonstrate the process characteristics primarily in terms of the geometrical features. A preliminary study to was conducted to determine the feasibility regions, which is not detailed here for brevity. After these preliminary tests, pulse repetition rate (*PRR*), wire feeding angle ($\alpha$) and direction, wire feed rate (*WFR*) were fixed at suitable levels allowing for a stable process. Then, the experimental study was conducted in two distinct parts, single and multi-layer deposition to produce thin-walled structures respectively. Designed experiments were used in both cases and different geometrical characteristics were the measured response variables. These features were analysed separately, despite a possible correlation between them. This is due to the fact that the work aims to illustrate and provide process maps showing the dimensional ranges of the measured geometrical features rather than a complete optimization.

**Table 3. Fixed and varied parameters in the study of single-layer deposition experiments.**

| **Fixed parameters** | **Level** |
|---|---|
| Spot diameter, $d_s$ (mm) | 0.85 |
| Pulse repetition rate, PRR (Hz) | 7 |
| Wire feeding angle, α (°) | 30 |
| Wire feeding direction | Front |
| Wire feed rate, WFR (mm/min) | 230 |
| Shielding gas | Ar at 0.8 bar |

| **Varied parameters** | **Levels** | | | | |
|---|---|---|---|---|---|
| | a- | c- | 0 | c+ | a+ |
| Pulse energy, E (J) | 9 | 9.6 | 10.5 | 11.4 | 12 |
| Pulse duration, τ (ms) | 6 | 7.2 | 9 | 11 | 12 |
| Transverse speed, v (mm/min) | 90 | 108 | 135 | 162 | 180 |

**Table 4. Fixed and varied parameters in the study of multi-layer deposition experiments.**

| **Fixed parameters** | **Level** |
|---|---|
| Spot diameter, $d_s$ (mm) | 0.85 |
| Pulse repetition rate, PRR (Hz) | 7 |
| Wire feeding angle, α (°) | 30 |
| Wire feeding direction | Front |
| Wire feed rate, WFR (mm/min) | 230 |
| Shielding gas | Ar at 0.8 bar |
| Transverse speed, v (mm/min) | 162 |
| Number of layers, N | 40 |

| **Varied parameters** | **Levels** | | | | |
|---|---|---|---|---|---|
| | a- | c- | 0 | c+ | a+ |
| Pulse energy, E (J) | 9.8 | 10 | 10.25 | 10.5 | 10.7 |
| Pulse duration, τ (ms) | 6.8 | 7.2 | 7.6 | 8 | 8.6 |
| Height increment, Δz (mm) | 0.25 | 0.28 | 0.32 | 0.36 | 0.39 |

In the first part, single layer deposition was studied as function of pulse energy ($E$), pulse duration ($\tau$) and transverse speed ($v$). Deposit height ($H_1$) and width ($W$) were measured as shown in Figure 2. Dilution was calculated from the measurements using the following expression:

$$Dil = \frac{H_2}{H_1+H_2} \cdot 100 \quad (4)$$

where $H_2$ is the penetration depth into the substrate [22]. Deposited section ($A_d$) was also measured. In the second part, multi-layer deposition was studied with fixed transverse speed ($v$), while pulse energy ($E$), pulse duration ($\tau$) and height increment ($\Delta z$) were varied. In both phases, central composite design (CCD) with three factors was chosen as the experimental design. Corner (c) and axial (a) points were replicated twice, while central point (0) was replicated 6 times. The results of single-layer deposition were used to set multiple-layer deposition parameters. A narrower range of pulse energy and pulse duration was employed for multi-layer deposition, while the transverse speed was fixed at 162 mm/min, which allowed for stable operation in multiple layers. A total of 40 layers ($N$) was deposited. The average height ($H_{av}$) and width ($W_{av}$) were measured with a height gauge and coordinate measuring machine (CMM) respectively. Cross-sections of the produced thin-wall structures were taken to measure Vickers microhardness (HV) and deposited section ($A_d$). Details of the experimental plans in single-layer and multi-layer deposition studies are summarized in Table 3 and Table 4 respectively. For investigated response variables regression models were sought. The statistical significance level was set at 5%. Residuals were checked for homogeneity and normality. The goodness of fit was evaluated through $R^2_{adj}$ and lack-of-fit was avoided in all models.

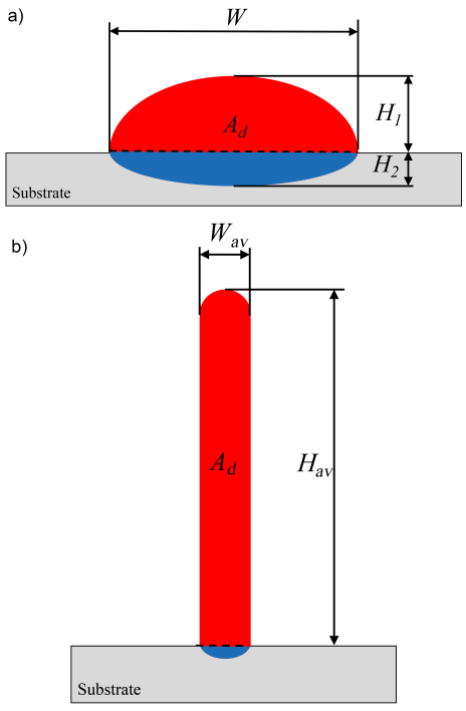


**Figure 2. Measurements taken on a) single and b) multi-layered depositions.**

## 3. Results

### 3.1. Single-layer deposition

Figure 3 reports cross-section images of the obtained single-layer deposits positioned in the parameter space of the CCD experimental plan. In general, it can be seen that the process yields limited amount of penetration, depicting a process based on conduction [23]. The microstructure depicts columnar grains grown at a perpendicular direction to the substrate plane, following the main direction of conduction. The micrographs also depict complete microstructural change on the deposited material in all the experimented conditions, confirming that the laser provided sufficient energy for melting. The penetration depth appears to be minimal in conditions with low energy content, high pulse duration and high speed. However, complete adhesion was present at all conditions. This is also confirmed after the cutting process involved for cross-section preparation, after which the specimens did not disintegrate.

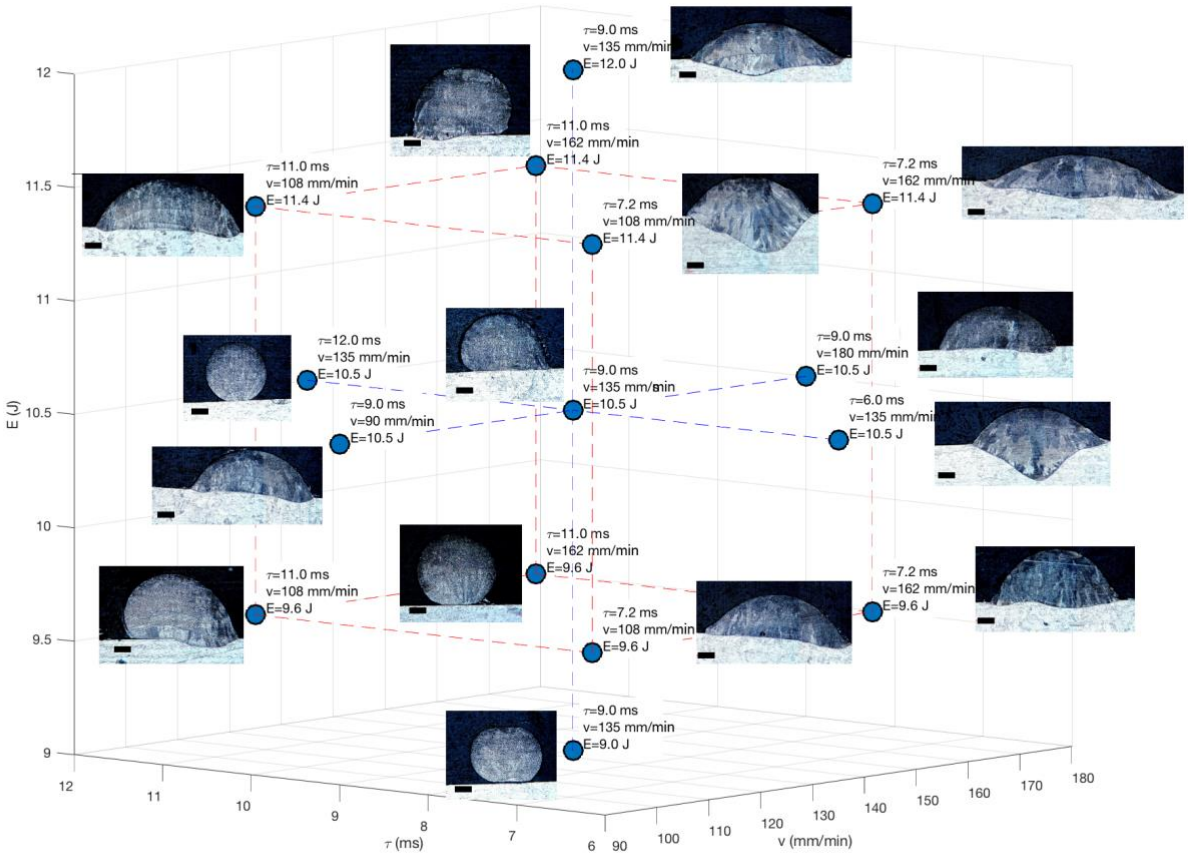


**Figure 3. Cross-section images of the single-track depositions as function of process parameters. Markers depict 100 μm.**

The fitted regression models allow for a better comprehension of the effect of the process parameters on deposit height ($H_1$) and width ($W$). In the case of the deposit height the model consisted of first order parameters and second order of transverse speed ($v$) as expressed in the following equation.

$$H_1\ (\mu m)\ =\ -35.37 \cdot E(J)\ + 27.27 \cdot \tau(ms)\ + 7.06 \cdot v(mm/min)\ - 0.025 \cdot\ [v(mm/min)]^2 \quad (5)$$

The model fitted the data adequately with $R_{2adj}$ at 98.71%. Figure 4 reports the contour plots of the regression model. It can be seen that the deposit height varied in a rage below the wire diameter between 150 and 500 μm. Higher pulse duration ($\tau$) and lower pulse energy ($E$) produce higher deposits at single layer level. These conditions correspond to lower pulse peak power ($P_{peak}$), since for square shaped laser pulses pulse energy is $P_{peak} = E/\tau$.

The effect of transverse speed ($v$) can be viewed at the different panels of Figure 4. The second order relationship accounts for an increase of deposit height at intermediate transverse speed levels, whereas both lower and higher transverse speed result in slight reduction of the deposit height. It can be expected that at high transverse speed levels deposit height is reduced due to the lower amount of material feed to the process zone. On the other hand, at low transverse speeds material can be lost due to higher amount of energy being delivered to the same zone, which results in material vaporization. For thin-walled structure manufacturing the deposit layer height plays an important role in the overall structure height as well as wall surface roughness over the build direction. For a faster production, higher deposits can be beneficial. On the other hand, this reduces the process resolution in build direction due to thicker layers used. Consequently, surface roughness can be increased.

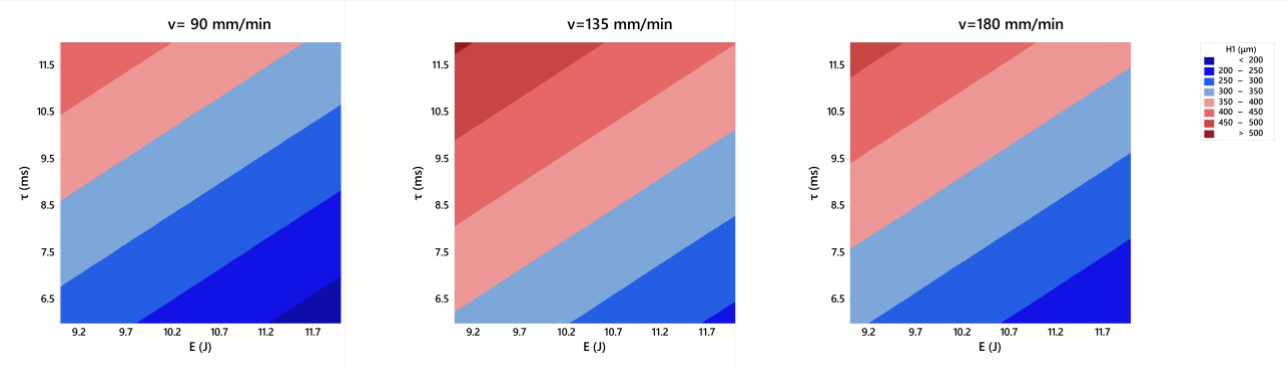


**Figure 4. Contour plots of deposit height at single track ($H_1$) as function of process parameters.**

In the case of deposit width, the regression equation consisted of pulse energy and pulse duration terms.

$$W\ (\mu m)\ =\ 153 \cdot E(J)\ - 82.6 \cdot \tau(ms) \quad (6)$$

The equation was found to fit the data well with $R2_{adj}$ at 97.03%. Figure 5 depicts the contour plot of the regression equation. It can be seen that the deposit width varies between 400 and 1200 µm. Opposite to the deposit height change, pulse duration ($\tau$) decreases the deposit width, whereas pulse energy ($E$) increases it. On the other hand, transverse speed ($v$) does not appear to influence deposit width significantly. Considered together with the deposit height, the change in deposit width indicates that higher pulse peak power ($P_{peak}$) results in low aspect ratio. The role of deposit with in thin-walled structure manufacturing is evidently related to the overall structure width. As a matter of fact, in the tested region deposit width can exceed 1 mm, corresponding to structure width more than twice the wire diameter.

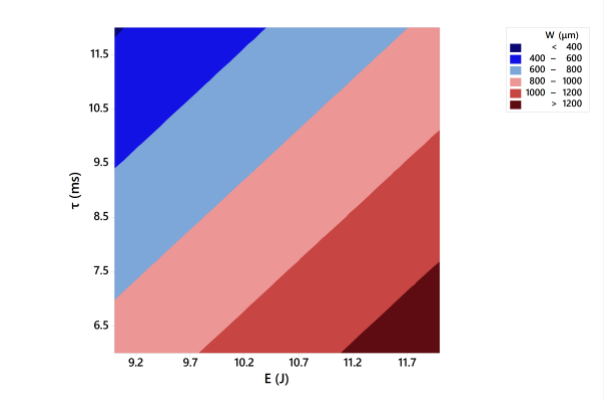


**Figure 5. Contour plots of deposit width at single track ($W$) as a function of process parameters.**

Similar to track width, the regression model of dilution ($Dil$) consisted of first order pulse energy ($E$) and pulse duration ($\tau$) terms.

$$Dil(\%) = 7.259 \cdot E(J) - 6.5 \cdot \tau(ms) \quad (7)$$

The model fit the data well with $R2_{adj}$ at 85.19%. Figure 6 reports the contour plot of the model. It can be seen that dilution was below 50% within the experimented range and followed a similar trend to that of deposit width. Increased pulse energy ($E$) and decreased pulse duration ($\tau$) result in higher dilution. Also in this case, transverse speed ($v$) does not induce any significant change over the response variable. Considered together with the deposit height and width, the observations over dilution imply that transverse speed mainly influences the amount of material feed over the substrate, which can be deposited effectively or lost from the surface. The role of dilution in thin-walled structure manufacturing is essential in the first layer for anchoring the rest of the built structure to the substrate. From this point of view a limited amount of dilution (<10%) is sufficient. Accordingly, in the multi-layer deposition phase the transverse speed was fixed at an intermediate value of

162 mm/min, which also provided stable deposition conditions in multi-layer conditions. In order to ensure sufficient dilution without an excessive width increase both pulse energy and duration were varied in a narrower range.

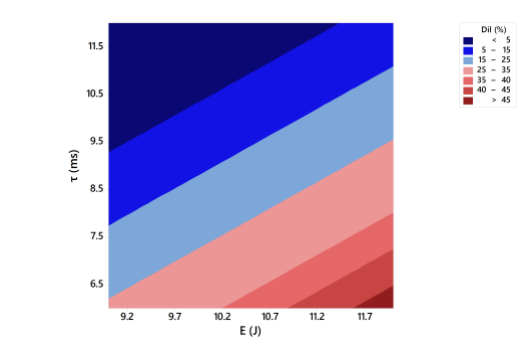


**Figure 6. Contour plots of dilution at track (*Dil*) as function of process parameters.**

### 3.2. Multi-layer deposition and thin wall manufacturing

Figure 7 depicts examples of multi-layer deposition of thin walls. A common problem in DED processes related to the difference between effective layer height ($\Delta H$) and height increment ($\Delta z$) manifests also in μWLMD. Stable conditions without a mismatch between $\Delta H$ and $\Delta z$ exhibit regular walls in all three dimensions and high aspect ratio structures are obtained (Figure 7.a). In conditions where effective layer height is lower than height increment ($\Delta H < \Delta z$), wire detachment is observed at higher layers, resulting in intermittent deposition (Figure 7.b). On the other hand, when effective layer height is higher than height increment ($\Delta H > \Delta z$) wire stability is lost due to collision between the nozzle and the built structure, which generates deposition loss at the initial part of the layer (Figure 7.b). Accordingly, average height ($H_{av}$) was analysed on all samples on the stable deposition regions, whereas the samples with the previously described defects were not included in further analysis.

The regression model for average height ($H_{av}$) consisted of first and second order terms of all the three process parameters.

$$H_{av}\,(mm) = 6.92 \cdot E(J) - 5.10 \cdot \tau(ms) - 34.4 \cdot \Delta z(mm) - 0.3592 \cdot [E(J)]^2 + 0.336 \cdot \tau[(ms)]^2 + 98.4 \cdot [\Delta z(mm)]^2 \quad (8)$$

The model was found to fit the data well with $R_{2adj}$ at 99.97%. Figure 9 reports the contour plots of the model. Within the experimented region average height varied between 11 and 15.5 mm with 40 layers of deposition.

The average height follows a very similar trend to that of deposit height ($H_1$) at single layer. Increased pulse energy ($E$) results in lower average height. Pulse duration ($\tau$) provides increase over average height. The most remarkable effect is provided by the height increment ($\Delta z$), which is directly associated to the total height travelled by the machine axis. Besides, for the given material and wire diameter combination the most suitable region was for height increment ($\Delta z$) found to be between 0.32 and 0.36 mm in order to avoid the reported defects.

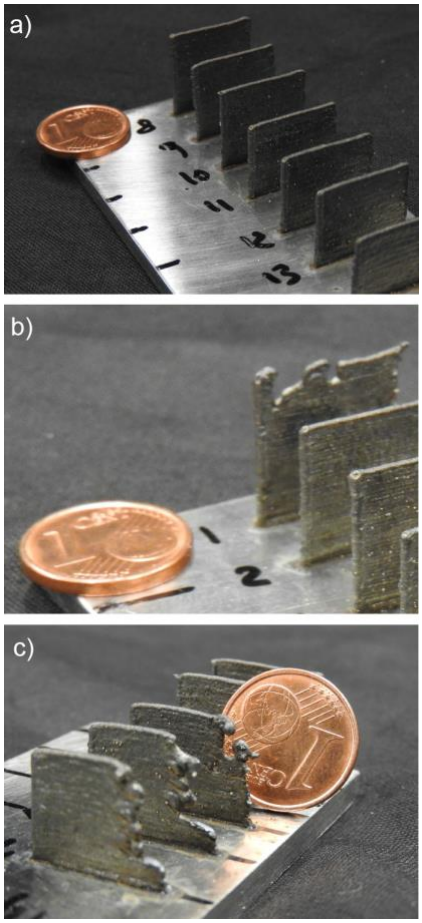


**Figure 7. Examples of manufactured thin walls showing high quality conditions without geometrical errors and mismatch between effective layer height and height increment. a) Conditions without geometrical errors, b) effective layer height lower than height increment ($\Delta H < \Delta z$), c) effective layer height higher than height increment ($\Delta H > \Delta z$).**

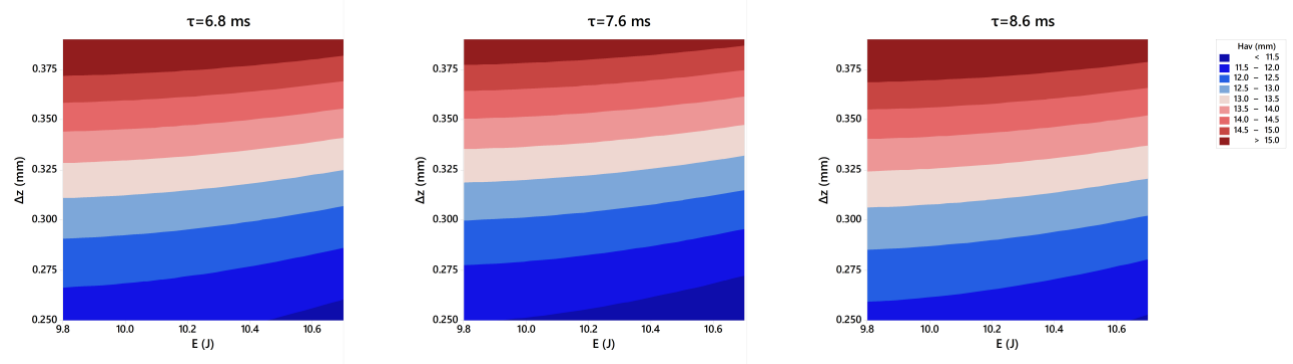


**Figure 8. Contour plots of thin wall structure height ($H_{av}$) as function of process parameters.**

The regression equation for average width ($W_{av}$) consisted of first order terms of pulse energy ($E$) and height increment ($\Delta z$) as well as the second order term of pulse energy.

$$W_{av}\ (mm)\ =\ 0.2604 \cdot E(J)\ -1.455 \cdot \Delta z(mm)\ -0.01282 \cdot [E(J)]^2 \quad (9)$$

The model was found to fit the data well as demonstrated by $R_{2adj}$ at 99.95%. Figure 9 shows the contour plot of the fitted model. In the experimented region, the widths of the deposits varied between 0.75 and 0.85 mm, maintaining dimensions comparable to the wire diameter. The effect of pulse energy ($E$) appears to be limited, which providing a slight increase towards intermediate values and a slight decrease towards higher ones. The effect of height increment ($\Delta z$) is more pronounced. Evaluated together with average height, the decrease in average width is a consequence of the distribution of the deposited layer over layer height rather than width.

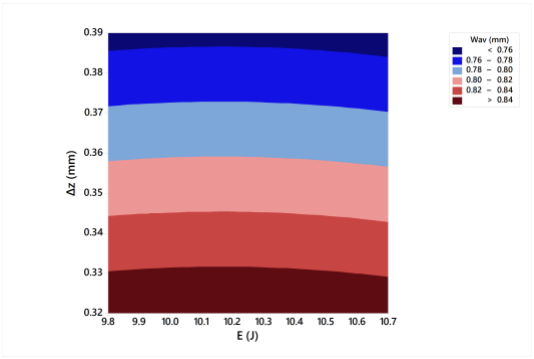


**Figure 9. Contour plots of thin wall structure width ($W_{av}$) as function of process parameters.**

In order to analyse material integrity after the deposition process micrograph analyses and microhardness measurements were carried out on cross-sections. No pores were found on all the analysed specimens and the hardness profile did not differ as function of process parameters. Figure 10 reports the average hardness profile of the realized thin walls as function of position over the build direction. The inset of Figure 10 exhibits cross-section image of a representative condition. It can be seen that consecutive layers are placed correctly positioned over each other and each layer is in a rectangular form. The rectangular layer form implies that consecutive layers provide partial melting over the previous ones partially flattening them. The hardness profile shows that hardness increases around the substrate-thin wall interface to approximately 220 HV. The higher microhardness values are attributed to the finer microstructure achieved by the end of the process. Thin wall hardness profile reaches a stable value at approximately 190 HV around 2 mm height. The substrate hardness on the other hand is approximately 140 HV. The hardness profile indicates that homogenous material mechanical properties are present over the build direction.

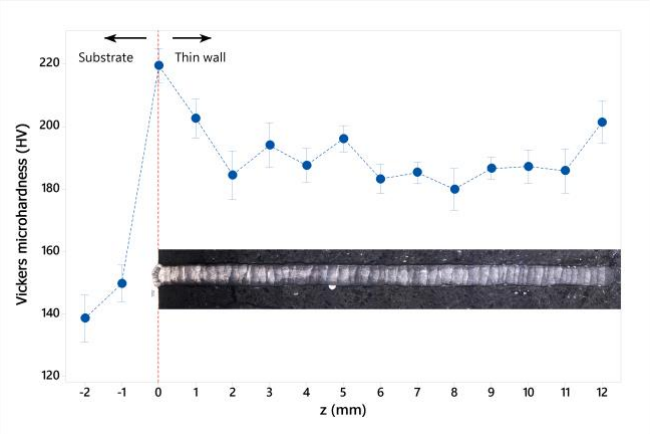


**Figure 10. Microhardness profiles of produced thin walls. The inset image shows an example of cross-section of the deposited thin wall (error bars represent 95% confidence interval for the mean).**

Despite the promising results, a further investigation of the material mechanical properties is required to assess a homogenous behaviour especially in the z direction [24]. Tensile specimens produced in different build inclinations should be produced and tested for static and fatigue properties. As a more detailed analysis, digital image correlation methods can be exploited to observe the behavior of the layered material under different loading conditions [25].

### 3.3. Material use efficiency

Material use efficiency ($\eta$) was evaluated for single and multi-layer depositions separately. For single layer depositions efficiency varied between 0.5 and 0.9. In multiple-layer deposition only the specimens without defected conditions were analysed, and a significant increase was observed between 0.95 and 0.99. In order to evaluate the effect of the delivered energy intensity over the material use efficiency fluence was used as a descriptive parameter, described by the following equation.

$$F = \frac{E \cdot PRR}{d_s \cdot v} \tag{10}$$

Regression models could be fitted to describe the evolution of material use efficiency as function of fluence for single and multi-layer depositions. In both cases the model form remained the same, where $\eta$ was inversely proportional to $F$. For single layer deposition regression equation was:

$$\eta = 22/F\ (J/mm^2) \tag{11}$$

with $R_{2adj}$=98.23%, while for multi-layer deposition,

$$\eta = 30/F\ (J/mm^2) \tag{12}$$

with $R_{2adj}$=99.94%. The fitted curves are demonstrated in Figure 11. The main implication of these results is that within the stable deposition conditions μWLMD yields very high efficiency in material use. The reduction in material use efficiency with increased fluence can be directly linked to the increase of fume and vapour generation as well as sparks and dross, which were observed in the corresponding experimental conditions. The multi-layer deposition yields higher efficiency overall, which is also demonstrated by the higher coefficient of the single regressor. It should be noted that multi-layer deposition was found to function stably in reduced pulse energy and pulse duration regions, hence the overall fluence region is limited (30-32.5 J/mm2) and is at the lower end of the fluence region of the single-layer conditions (27-57 J/mm2). Moreover, dilution between the substrate and deposited layer is only present at the first layer, which can reduce material use efficiency due to the mixing between the two materials.

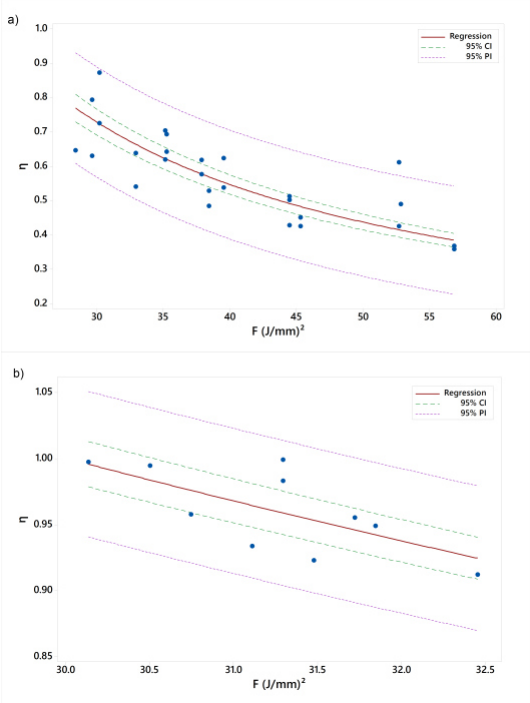


**Figure 11. Deposition efficiency ($\eta$) as function of fluence for a) single layer and b) multi-layer deposition.**

### 3.4. Manufacturing of thin-walled structures

In order to demonstrate the capability of the developed process, thin-walled structures were produced, which are demonstrated in Figure 12. The wings depicted in Figure 12.a and b demonstrate the possibility of inclined wall production with different inclination angles against the build direction and deposition direction. In particular, freestanding structures with inclinations down to 58° with respect

to the build substrate could be achieved both along the deposition direction and between the layers. Axisymmetric parts are highly suitable for DED processes, which were also used as demonstrator cases. The rotational axis of the welding station was employed for the purpose. Figure 12.c shows a tube with constant thickness and diameter. A layer-by-layer deposition strategy was employed, where the height increment was applied at the end of each layer. In Figure 12.d a conical shape is shown, demonstrating the possibility of diameter variation along the build axis. The demonstrator piece was produced by applying a height increment and radial displacement between layers.

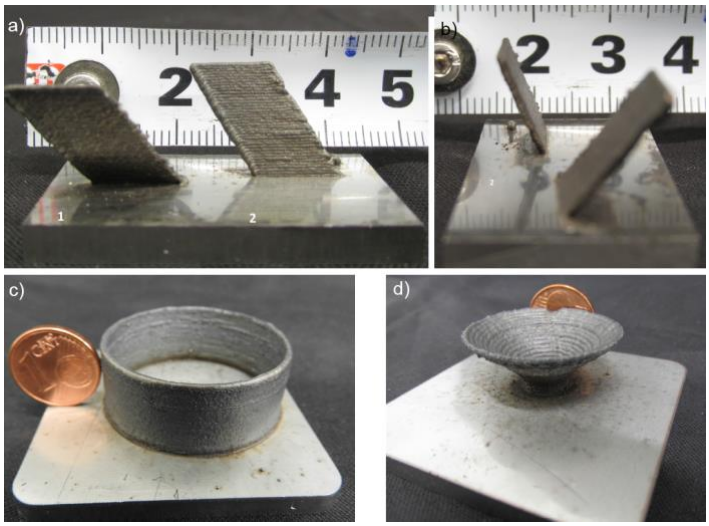


**Figure 12. Additive manufacturing of thin-walled structures. a,b) Inclined walls with 13 mm height at 58° and 69° inclination angles with respect to the substrate plane ; c) tube with 13 mm height and 35 mm diameter; and d) cone with 10 mm height.**

## 4. Conclusions

In this work micro laser metal wire deposition has been developed. Wire based DED processes mainly aim for high deposition rates, whereas the present study investigated the possibility of achieving reduced dimensions and improved geometrical tolerances by the use of laser-wire combination. The system composed of a pulsed Nd:YAG laser as the heat source and an in-house build wire feeder system synchronised with the numerical control of a laser welding station. For increased dimensional resolution 0.5 mm wires of AISI 301 stainless steel were investigated. The main conclusions of this work can be summarized as the following.

- Pulsed wave laser emission at 1 μm wavelength and ms range pulse durations provide suitable melting conditions of the wire based on condition.

- At single-layer level high pulse energy and pulse duration result in wider and shorter layer height, as well as higher dilution. The processing conditions may increase the layer width to dimensions larger than twice the wire diameter, which should be regulated to maintain micrometric dimensions. Transverse speed on the other hand may reduce the amount of material deposited at high and low ranges, whereas intermediate values are highly suitable to maintain stable process.
- In multi-layer deposition, height increment of the deposition system should match the effective layer height. Mismatched conditions result in irregular depositions.
- Thin-walled structures with layer widths between 700 and 800 µm and layer height between 300-375 µm could be realized. Such layer widths were maintained over 15 mm total build height corresponding to an aspect ratio of approximately 20.
- The process generates homogenous material properties over the build direction as observed by the microhardness measurements.
- The process yields very high material use efficiency. Material use efficiency is reduced by high fluence levels due to vapour and spark generation. In stable deposition conditions such phenomena are avoided.
- Demonstrator cases showed that the process can be suitably employed to additively manufacture different thin-walled shapes employing wall inclinations and section changes.
- In terms of dimensional range the µWLMD process can be positioned as a solution between powder bed and directed energy deposition additive manufacturing processes. Amongst the wire based additive manufacturing processes it stands out as the one providing smallest dimensions.

The µWLMD process can be further developed to reduce dimensions by the use of thinner wires and positioning systems with higher accuracy. The laser-material interaction should be further investigated with thinner wires and their mechanical stability during the wire feed should be assessed. One of the main limitations of the process is the monodirectional deposition capability due to the optical arrangement and wire feed direction. System improvements regarding this aspect would be beneficial. The effect on different materials and the influence of wire properties on the process quality require further attention within future research.

**Acknowledgements**

The author wishes to express his gratitude to Martina Riccio and Eligio Grossi for their contribution to the system development and experimental work and Prof. Barbara Previtali for the valuable technical discussion. This work was supported by Regione Lombardia under the call “Creatività: Eventi e Luoghi per L’innovazione nella Moda e nel Design, Linea 2: Infrastrutturazione Fisica e Digitale”.

**References**


[1] ASTM International. F2792-12a - Standard Terminology for Additive Manufacturing Technologies. Rapid Manuf Assoc 2013:10–2. doi:10.1520/F2792-12A.2.

[2] Ding D, Pan Z, Cuiuri D, Li H. Wire-feed additive manufacturing of metal components: technologies, developments and future interests. Int J Adv Manuf Technol 2015;81:465–81. doi:10.1007/s00170-015-7077-3.

[3] Tang Q, Pang S, Chen B, Suo H, Zhou J. A three dimensional transient model for heat transfer and fluid flow of weld pool during electron beam freeform fabrication of Ti-6-Al-4-V alloy. Int J Heat Mass Transf 2014;78:203–15. doi:10.1016/j.ijheatmasstransfer.2014.06.048.

[4] Heralić A, Christiansson A-K, Lennartson B. Height control of laser metal-wire deposition based on iterative learning control and 3D scanning. Opt Lasers Eng 2012;50:1230–41. doi:http://dx.doi.org/10.1016/j.optlaseng.2012.03.016.

[5] Murr LE, Gaytan SM, Ramirez D a., Martinez E, Hernandez J, Amato KN, et al. Metal Fabrication by Additive Manufacturing Using Laser and Electron Beam Melting Technologies. J Mater Sci Technol 2012;28:1–14. doi:10.1016/S1005-0302(12)60016-4.

[6] Slotwinski JA, Garboczi EJ, Stutzman PE, Ferraris CF, Watson SS, Peltz MA. Characterization of Metal Powders Used for Additive Manufacturing. J Res Natl Inst Stand Technol 2014;119:460–93. doi:10.6028/jres.119.018.

[7] Yan C, Hao L, Hussein A, Young P, Raymont D. Advanced lightweight 316L stainless steel cellular lattice structures fabricated via selective laser melting. Mater Des 2014;55:533–41. doi:10.1016/j.matdes.2013.10.027.

[8] Stamp R, Fox P, O'Neill W, Jones E, Sutcliffe C. The development of a scanning strategy for the manufacture of porous biomaterials by selective laser melting. J Mater Sci Mater Med 2009;20:1839–48. doi:10.1007/s10856-009-3763-8.

[9] Kim JD, Kang KH, Kim JN. Nd?:?YAG laser cladding of marine propeller with hastelloy C-22. Appl

Phys A 2004;79:1583–5. doi:10.1007/s00339-004-2854-0.

[10] Kim J Do, Peng Y. Melt pool shape and dilution of laser cladding with wire feeding. J Mater Process Technol 2000;104:284–93. doi:10.1016/S0924-0136(00)00528-8.

[11] Kim J Do, Peng Y. Plunging method for Nd:YAG laser cladding with wire feeding. Opt Lasers Eng 2000;33:299–309. doi:10.1016/S0143-8166(00)00046-4.

[12] Hussein NIS, Segal J, McCartney DG, Pashby IR. Microstructure formation in Waspaloy multilayer builds following direct metal deposition with laser and wire. Mater Sci Eng A 2008;497:260–9. doi:10.1016/j.msea.2008.07.021.

[13] Syed WUH, Pinkerton AJ, Li L. Combining wire and coaxial powder feeding in laser direct metal deposition for rapid prototyping. Appl Surf Sci 2006;252:4803–8. doi:10.1016/j.apsusc.2005.08.118.

[14] Mumtaz, Kamran Aamir; Hopkinson N. Selective Laser Melting of Inconel 625 Using Pulse Shaping. Rapid Prototyp J 2010;16:165–78. doi:10.1108/13552541080000463.

[15] Martina F, Mehnen J, Williams SW, Colegrove P, Wang F. Investigation of the benefits of plasma deposition for the additive layer manufacture of Ti-6Al-4V. J Mater Process Technol 2012;212:1377–86. doi:10.1016/j.jmatprotec.2012.02.002.

[16] Jhavar S, Jain NK, Paul CP. Development of micro-plasma transferred arc (μ-PTA) wire deposition process for additive layer manufacturing applications. J Mater Process Technol 2014;214:1102–10. doi:10.1016/j.jmatprotec.2013.12.016.

[17] Assuncao E, Williams S. Comparison of continuous wave and pulsed wave laser welding effects. Opt Lasers Eng 2013;51:674–80. doi:10.1016/j.optlaseng.2013.01.007.

[18] Capello E, Previtali B. The influence of operator skills, process parameters and materials on clad shape in repair using laser cladding by wire. J Mater Process Technol 2006;174:223–32. doi:10.1016/j.jmatprotec.2006.01.005.

[19] Washko S.D., Aggen G. Wrought Stainless Steels. ASM Handbook, Vol. 1, ASM International; 1990,

p. 841–907.

[20] Lin J. Simple model of powder catchment in coaxial laser cladding. Opt Laser Technol 1999;31:233–8. doi:10.1016/S0030-3992(99)00046-8.

[21] Le Bourhis F, Kerbrat O, Hascoet J-Y, Mognol P. Sustainable manufacturing: evaluation and modeling of environmental impacts in additive manufacturing. Int J Adv Manuf Technol 2013;69:1927–39. doi:10.1007/s00170-013-5151-2.

[22] Capello E, Colombo D, Previtali B. Repairing of sintered tools using laser cladding by wire. J Mater Process Technol 2005;164–165:990–1000. doi:10.1016/j.jmatprotec.2005.02.075.

[23] Assuncao E, Williams S, Yapp D. Interaction time and beam diameter effects on the conduction mode limit. Opt Lasers Eng 2012;50:823–8. doi:10.1016/j.optlaseng.2012.02.001.

[24] Baufeld B, Brandl E, Van Der Biest O. Wire based additive layer manufacturing: Comparison of microstructure and mechanical properties of Ti-6Al-4V components fabricated by laser-beam deposition and shaped metal deposition. J Mater Process Technol 2011;211:1146–58. doi:10.1016/j.jmatprotec.2011.01.018.

[25] Pan B, Asundi A, Xie H, Gao J. Digital image correlation using iterative least squares and pointwise least squares for displacement field and strain field measurements 2009;47:865–74. doi:10.1016/j.optlaseng.2008.10.014.

**List of figures**



**List of tables**